

Estimating Nonlinearities in p-Linear Hyperspectral Mixtures

Andrea Marinoni¹, Senior Member, IEEE, Javier Plaza², Senior Member, IEEE,
Antonio Plaza², Fellow, IEEE, and Paolo Gamba¹, Fellow, IEEE

Abstract—Accurately estimating the elements in Earth observations is crucial when assessing specific features such as air quality index, water pollution, or urbanization process behavior. Moreover, physical–chemical composition can be retrieved from hyperspectral images when proper spectral unmixing architectures are employed. Specifically, when linear and nonlinear combinations of endmembers (pure spectral components) are accurately characterized, hyperspectral unmixing plays a key role in understanding and quantifying phenomena occurring over the instantaneous field-of-view. Thus, reliable detection of nonlinear reflectance behavior can play a key role in enhancing hyperspectral unmixing performance. In this paper, two new methods for adaptive design of mixture models for hyperspectral unmixing are introduced. One of the methods relies on exploiting geometrical features of hyperspectral signatures in terms of nonorthogonal projections onto the space induced by the endmembers' spectra. Then, an iterative process aims at understanding the order of local nonlinearity that is displayed by each endmember over every pixel. An improved version of an artificial neural network-based approach for nonlinearity order information is also considered and compared. Experimental results show that the proposed approaches are actually able to retrieve thorough information on the nature of the nonlinear effects over the image, while providing excellent performance in reconstructing the given data sets.

Index Terms—Adaptive fitting, iterative nonlinearity detection, nonlinear hyperspectral unmixing, nonorthogonal projection.

I. INTRODUCTION

HYPERSPECTRAL imagery provides a huge amount of information about spectral features of the earth surface [1]–[8]. Specifically, physical composition and anthropogenic phenomena (such as urbanization processes, air pollution, and water quality and distribution [9], [10]) can be detailed by appropriately estimating the fractions of the materials and elements (*endmembers*) appearing at each location [11].

Manuscript received May 25, 2017; revised October 5, 2017 and January 13, 2018; accepted May 13, 2018. Date of publication June 21, 2018; date of current version October 25, 2018. (*Corresponding author: Andrea Marinoni.*)

A. Marinoni and P. Gamba are with the Telecommunications and Remote Sensing Lab, Department of Electrical, Computer and Biomedical Engineering, University of Pavia, I-27100 Pavia, Italy (e-mail: andrea.marinoni@unipv.it; paolo.gamba@unipv.it).

J. Plaza and A. Plaza are with the Hyperspectral Computing Laboratory, Department of Computer Technology and Communications, University of Extremadura, E-10071 Cáceres, Spain (e-mail: jplaza@unex.es; aplaza@unex.es).

Color versions of one or more of the figures in this paper are available online at <http://ieeexplore.ieee.org>.

Digital Object Identifier 10.1109/TGRS.2018.2840524

Hyperspectral unmixing aims at characterizing a scene by inverting (*unmixing*) models that describe the mixture of the elements. In order to deal with the nonlinear spectral variety of the hyperspectral signatures induced by their low spatial resolution, mixture models relying on the sparsity of the endmember set to perform unmixing have been considered [12]. In fact, methods that aim at characterizing the nonlinear effects of endmember combinations by promoting sparse mixing solutions have been proposed [13]–[15]. These models might effectively reconstruct the hyperspectral mixtures when the mixture model used to generate the endmember set spectrally and geometrically matches the scenario profile. Hence, they cannot adaptively describe the different sources of nonlinear effects in the hyperspectral target, leading to an eventual degradation on the performance of the architecture to understand and quantify the actual endmember combination and the elemental composition of the considered scenes.

Thus, several models take into consideration the complex physical interactions of the elements of the surface and involve nonlinear effects. For instance, in [16], a multilinear mixture model (multi-LMM) has been introduced. This scheme aims at characterizing linear and nonlinear interactions among the endmembers by properly minimizing a cost function, and detects the most likely type of mixture. The methods introduced in [17] and [18] can be also used to retrieve a feasible description of the effects that result from linear mixtures of endmembers. Specifically, they aim at identifying the additive term which is assumed to corrupt the linear mixture term. The expression of the corruption contribution can be adapted to account for a set of considered phenomena (e.g., endmember variability and mismodeling effects [17], [18]).

These aforesaid algorithms are able to detect and describe the nonlinearities affecting the pixel signatures. In order to deliver a feasible architecture and leverage computational complexity, they rely on probability estimation [16], kernel separability [17], and Bayesian inference [18]. This choice may represent a limit, and lead to solutions that are not completely detailing physical effects while being mathematically feasible.

On the contrary, several papers have recently addressed the topic of nonlinearity detection in hyperspectral images according to macroscopic mixture modeling. For instance, *a posteriori* statistical tests have been used to understand bilinearity in [19]–[21]. In [11], a semisupervised approach to address higher order nonlinearity detection has been proposed

by introducing a framework for efficient p -linear unmixing with a preprocessing step to estimate the nonlinearity order of each pixel. To this aim, an artificial neural network (ANN) is properly trained to perform an estimate of the order of the nonlinear interactions that occur over every pixel of the scene. This architecture delivers an effective improvement in hyperspectral unmixing performance, as it prevents overfitting. The downside of this approach is its computational complexity. Hence, there is room for more efficient methods for nonlinearity detection within hyperspectral images possibly based onto new strategies.

In this paper, a novel method for adaptive design of mixture models for hyperspectral unmixing is introduced. Specifically, the proposed approach relies on exploiting the geometrical features of hyperspectral signatures in terms of nonorthogonal projections onto the space induced by the endmember spectra to select whether the mixture is linear or nonlinear. Then, an iterative process used to understand the order of the local nonlinearity by each endmember over every pixel. In addition, an improved version of the original ANN-based nonlinearity order information is considered and compared. Experimental results show that both newly developed approaches are able to retrieve enough information about the nature of the nonlinear effects over the image while providing excellent performance in reconstructing the given data sets.

The remainder of the paper is organized as follows: Section II describes the proposed methods, while Section III analyzes the experimental results. Finally, Section IV provides the conclusions of this paper and some final remarks.

II. METHODS

In this Section, two methods to estimate the order of the non-LMM are presented. Specifically, these methods aim at identifying the parameters of a multiple p -LMM (mpLMM)

$$\underline{y}_l = \sum_{r=1}^R \hat{a}'_{lr} \underline{m}_r + \sum_{r'=1}^R \sum_{k'=2}^{p_{r'}} \hat{\beta}'_{lr'k'} \underline{m}_{r'}^{k'} + \hat{n}'_l \quad (1)$$

where $\underline{y}_l = [y_{ln}]_{n=1, \dots, N}$ is the N -band spectral signature of the l th pixel that is part of a P -pixel image. Moreover, $\underline{m}_r = [m_{rn}]_{n=1, \dots, N}$ is the spectral signature of the r th endmember, and $\underline{m}_r^k = [m_{rn}^k]_{n=1, \dots, N}$. $\hat{a}'_{lr} = [\hat{a}'_{lr}]_{r=1, \dots, R}$ and $\hat{\beta}'_{lr'} = [\hat{\beta}'_{lr'}]_{r=1, \dots, R}$ are the coefficients that drive the linear and nonlinear mixture, respectively, i.e., $\sum_{r=1}^R \hat{a}'_{lr} + \sum_{r'=1}^R \hat{\beta}'_{lr'} = 1$, $\hat{a}'_{lr} \geq 0 \forall r$, $\hat{\beta}'_{lr'} \geq 0 \forall r'$.

In this formula, $p_{r'}$ identifies the order of the r' th endmember's contribution to the nonlinear mixture of the l th pixel, and the proposed methods are able to estimate it. Specifically, in Section II-A, a scheme based on iterative nonorthogonal projection process is reported, while Section II-B introduces an approach based on ANNs.

A. Estimating Nonlinearity Orders by Nonorthogonal Projection

The first approach is based on the nonorthogonal projection (N.O.Pro) estimate introduced in [22] with important and novel additions (highlighted by the red box in Fig. 1).

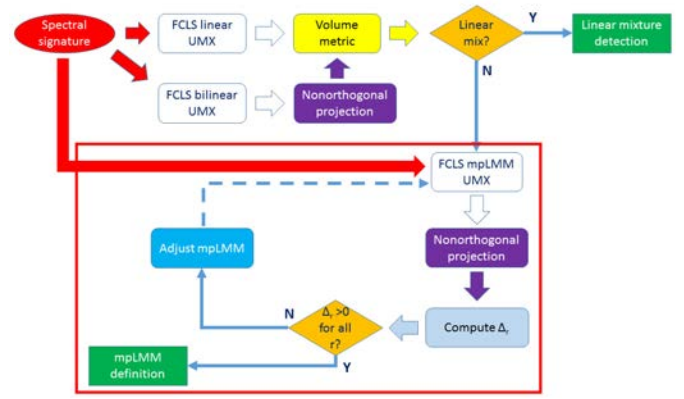


Fig. 1. Basic workflow of the framework for linear mixture detection introduced in [22], with the proposed scheme for nonlinearity order estimation reported in Section II-A highlighted in the red box.

This architecture (named N.O.Pro., according to the main technique it employs) exploits fully constrained least squares (FCLS) algorithm to first detect the linear mixtures in the considered image. Specifically, we first run FCLS on the l th pixel \underline{y}_l to decompose it as a combination of the linear contributions of the endmembers, i.e., $\underline{y}_l = \hat{\underline{y}}_l^{(L)} + \hat{\underline{n}}_l = \sum_{r=1}^R \hat{a}'_{lr} \underline{m}_r + \hat{\underline{n}}_l$. We also use FCLS to identify the role of linear and bilinear contributions of the endmembers in the \underline{y}_l signature, i.e., $\underline{y}_l = \hat{\underline{y}}_l^{(L)} + \hat{\underline{y}}_l^{(NL)} + \hat{\underline{n}}_l = \sum_{r=1}^R \hat{a}'_{lr} \underline{m}_r + \sum_{r'=1}^R \hat{\beta}'_{lr'} \underline{m}_{r'}^2 + \hat{\underline{n}}_l$. In the aforesaid equations, the a , a' and β' terms identify the coefficients that drive the linear and bilinear mixtures as computed by FCLS. Moreover, $\hat{\underline{n}}$ and $\hat{\underline{n}}'$ are the noise residuals obtained from the FCLS linear and bilinear unmixing, respectively. Please also note that the notation in the aforesaid equations is different to emphasize the difference among the coefficients retrieved by FCLS in those two situations.

The method in [22] detects the linear mixtures by processing these coefficients. It basically relies on the difference between the distributions of the parameters in the aforementioned equations to estimate the nature of the mixtures in the scene. In the noiseless case, this information can be retrieved by the difference $\hat{\underline{y}}_l^{(L)} - \hat{\underline{y}}_l^{(NL)}$, which tends to 0 if the l th pixel results from a linear mixture of endmembers. On the other hand, when the noise-free scenario assumption does not hold, we need to design a more complex metric to assess the occurrence of linear mixtures in the image. To this aim, let us define $\hat{\underline{y}}_l^{(L)} - \hat{\underline{y}}_l^{(NL)} = \hat{\underline{D}}_l = \sum_{r=1}^R \hat{\delta}_{lr} \underline{m}_r$, where $\hat{\delta}_{lr} = \hat{a}_{lr} - \hat{a}'_{lr}$ and $\hat{\delta}_l = [\hat{\delta}_{lr}]_{r=1, \dots, R}$. Then, we can write $\hat{\underline{D}}_l = \hat{\underline{y}}_l^{(NL)} + \hat{\underline{d}}_l^{(n)} = \hat{\underline{y}}_l^{(NL)} + (\hat{\underline{n}}_l - \hat{\underline{n}}_l)$. This representation allows us to quantify the actual contribution of noise and nonlinear combinations of endmembers to the spectral signature of each pixel. The method in [22] introduces a metric based on volume distances computed on the polytopes induced by $\hat{\underline{D}}_l$, $\hat{\underline{y}}_l^{(NL)}$, and $\hat{\underline{d}}_l^{(n)}$ in the space spanned by $\mathcal{M} = \{\underline{m}_r\}_{r=1, \dots, R}$. This metric requires these quantities to be referred to the \mathcal{M} mutual vectorial field, such that the distance and difference definitions can be delivered according to Euclidean geometry, and volumes can be consistently computed.

In other terms, we aim to write $\hat{\mathcal{D}}_l = \sum_{r=1}^R \hat{\delta}_{lr} \underline{m}_r = \sum_{r=1}^R \pi_r(\hat{\underline{y}}_l^{(NL)}) \underline{m}_r + \sum_{r=1}^R \pi_r(\hat{\mathcal{D}}_l^{(n)}) \underline{m}_r$, where $\pi_r(\underline{z})$ identifies the nonorthogonal projection of \underline{z} onto the direction imposed by the r th endmember. Each term $\pi_r(\hat{\underline{y}}_l^{(NL)})$ and $\pi_r(\hat{\mathcal{D}}_l^{(n)})$ are to be computed by applying Clifford algebra and Cramer's rule to the \mathcal{M} -space [22]. Then, it is possible to compute the volume induced by the polytopes identified by $\hat{\mathcal{D}}_l$, $\underline{y}'_l = \sum_{r=1}^R \pi_r(\hat{\underline{y}}_l^{(NL)}) \underline{m}_r$, and $\underline{\mathcal{D}}_l^{(n)} = \sum_{r=1}^R \pi_r(\hat{\mathcal{D}}_l^{(n)}) \underline{m}_r$ in the \mathcal{M} -space according to the Cayley–Menger formula [23], [24]. Finally, the likelihood for linear mixture occurrence over the l th pixel is set as follows:

$$L_l = 1 - \frac{|V(\hat{\mathcal{D}}_l) - V(\underline{\mathcal{D}}_l^{(n)})|}{|V(\hat{\mathcal{D}}_l) - V(\underline{y}'_l)| + |V(\hat{\mathcal{D}}_l) - V(\underline{\mathcal{D}}_l^{(n)})|}. \quad (2)$$

Specifically, assuming uniform distribution to discriminate the linear and nonlinear mixtures, we can state that the l th pixel is assumed to result from a linear mixture of endmembers if $L_l > 0.5$. Therefore, recalling the workflow in Fig. 1, we step in the red box part when $L_l < 0.5$.

In order to proceed to understand the nonlinear contribution of each single endmember to the target spectral signature, we compute the distances of the projections over the r th endmember direction delivered by $\hat{\underline{y}}_l^{(NL)}$ and $\hat{\mathcal{D}}_l^{(n)}$ to $\hat{\delta}_{lr}$ as follows:

$$\Delta_r = |\hat{\delta}_{lr} - \pi_r(\hat{\underline{y}}_l^{(NL)})| - |\hat{\delta}_{lr} - \pi_r(\hat{\mathcal{D}}_l^{(n)})|. \quad (3)$$

Eventually, we can assume that the r th endmember is involved in the second-order nonlinear effects that gathered in \underline{y}_l if $\Delta_r < 0$ [22]. This scheme can be further improved beyond simply checking linear against bilinear mixtures. It aims at acquiring information on the actual order of the nonlinear effects that are driven by each endmember, the proposed approach can be iterated by extending the original set of endmembers and their square values with higher order contributions of the endmembers for which $\Delta_r < 0$. The general extension of this approach would turn into setting \mathcal{M}' at the k th step of the process to $\mathcal{M} \cup \overline{\mathcal{M}}^{(k)}$, where $\overline{\mathcal{M}}^{(k)}$ collects the k -linear contribution of the endmembers that have been considered as involved in the nonlinear effects at the $(k-1)$ th step, i.e., those for which $\Delta_r < 0$ at the $(k-1)$ th step. This process would iterate until $\Delta_r > 0 \forall r$. Table I reports the pseudocode of the proposed iterative structure.

B. ANN-Based Estimation of Nonlinear Orders

ANNs have been extensively exploited for hyperspectral analysis. In particular, feedforward networks (FNs) have been widely used in terms of classification and/or regression problems. Here, we use a standard FN with one single-hidden layer to estimate the nonlinearity order of the contribution of each endmember within each image pixel. This simple ANN has been proven to be very efficient due to its ability to approximate complex nonlinear mappings directly from the input samples [25].

Conjugate gradient algorithms have been proposed to perform a search along the conjugate directions, which generally

TABLE I
PSEUDOCODE OF THE ALGORITHM FOR ESTIMATION OF THE p_{lr} PARAMETERS IN (1) BY MEANS OF AN ITERATIVE NONORTHOGONAL PROJECTION PROCESS

```

Iterative nonorthogonal projections for estimation of nonlinearities in mpLMM
given a dataset  $\underline{y} = \{\underline{y}_l\}_{l=1, \dots, P}$  with  $P$  pixels and  $N$  bands;
set the endmember set  $\mathcal{M}$ ,  $|\mathcal{M}| = R$ ;
set  $p_{lr} = 2 \forall (l, r) \in \{1, \dots, P\} \times \{1, \dots, R\}$ ;
for  $l = 1$  to  $P$ 
  A   unmix  $\underline{y}_l$  according to LMM;
  B   unmix  $\underline{y}_l$  according to mpLMM based on the current  $p_{lr}$  setting  $\forall (l, r)$ ;
       $Z = 0$ ;
      for  $r = 1$  to  $R$ 
        compute  $\Delta_r$  as in (3);
        if  $\Delta_r < 0$ 
           $p_{lr} + 1 \rightarrow p_{lr}$ ;
        else
           $Z + 1 \rightarrow Z$ ;
        end if
      end for
      if  $Z < R$ 
        back to [B];
      else
        break;
      end if
end for

```

result in faster convergence than traditional gradient descent-based learning algorithms. Although they usually require higher storage capacity, they are widely used in networks with large number of weights. In particular, we adopted the scaled conjugate gradient learning algorithm, a variant of the conjugate gradient method, which avoids the line search per learning iteration by using a Levenberg–Marquardt approach in order to scale the step size [26].

The proposed ANN-based model to estimate the nonlinearity orders is then based on a very simple FN architecture composed of an input layer, one hidden layer, and an output layer. The node count in the input layer is fixed to the spectral dimensionality of the data (number of spectral bands of the considered data set). The number of output nodes equals the number of estimated endmembers in the data set, thus the target outputs of the network are the vectors with as many components as endmembers containing values in the set $\{0, 1, \dots, p_{lr}\}$, being p_{lr} the maximum possible order of nonlinearity. Finally, a logistic activation function is considered in the hidden layer.

A shortcoming of the proposed methodology for estimating the nonlinearity order is its supervised nature, together with the lack of available reference information for real images. It is then necessary to access a sufficient number of representative training samples which lead the model to produce accurate nonlinearity order estimations. In this sense, there exist some automatic training generation processes which have been published in the machine learning community. In particular, Okujeni *et al.* [27] and Suess *et al.* [28] present a strategy to use synthetically mixed training data for mapping subpixel land cover fractions with machine learning regression algorithms.

In this paper, we adopt a similar approach based on the synthetic generation of a representative set of training samples that

allow for a successful estimation of the mixture nonlinearity orders. The generation process only requires the extraction of the spectrally pure constituents (endmembers) of the image to be processed. With these endmembers, we automatically generate nonlinear mixtures (according to a specific model) with known nonlinearity orders, following a mixing systematic that is described in the following. These training patterns are used to train the neural network architecture. In order to generate the mixed training patterns, we need to define the following parameters.

- 1) *Pure Spectra*: as we have already mentioned, this is the only *a priori* information that we need from the image to be processed. For this purpose, we can use a variety of endmember extraction algorithms [3]. In particular, in this paper, we will use the well-known automated target generation process [29] for this purpose.
- 2) *Mixing Systematic*: To generate the nonlinear mixtures between the endmembers that will be used as training samples to feed the neural network, the first step is to select a mixture model. In this paper, we adopt the model defined by (1) to generate the spectral mixtures used for training purposes. Therefore, we need to specify the following aspects.
 - a) *Mixing Complexity*: this is related with the number of spectrally pure constituents available [R in (1)]. We need to decide the maximum of simultaneous different spectral signatures that will contribute to each mixture, and further analyze the effect of increasing this number of constituents in each mixture (i.e., binary, ternary, quaternary mixtures, etc.). It should be noted that the number of endmembers used in the mixtures R is not necessarily the same as the number of pure materials contributing to the mixture in each generated spectrum. It has been previously addressed in the literature that, in practice, a mixed pixel consists of four to five constituents at most [30], [31].
 - b) *Mixture Coefficients Sampling*: we also need to define a sampling strategy to generate the mixture coefficients \hat{a}'_{lr} and $\hat{b}'_{lr'k'}$, which determine the intermediate mixtures between pure spectra. In this sense, if the number of maximum different spectral signatures is less than the number of available endmembers (which is the usual situation), we need to perform all the combinations between the possible permutations with repetitions of maximum pure elements within the total number of endmembers. Fig. 2 shows all the possible permutations with repetitions of three different elements, considering a mixture increment/decrement of 25%. To generate the final training sample data set, it would be necessary to perform all the possible combinations of three elements (out of the whole set of available endmembers) satisfying these mixture coefficients. Then, we analyze the impact of this parameter in the final estimation produced by the ANN model.
 - c) *Mixing Nonlinearity Order Sampling*: this is related with the number of different nonlinearity

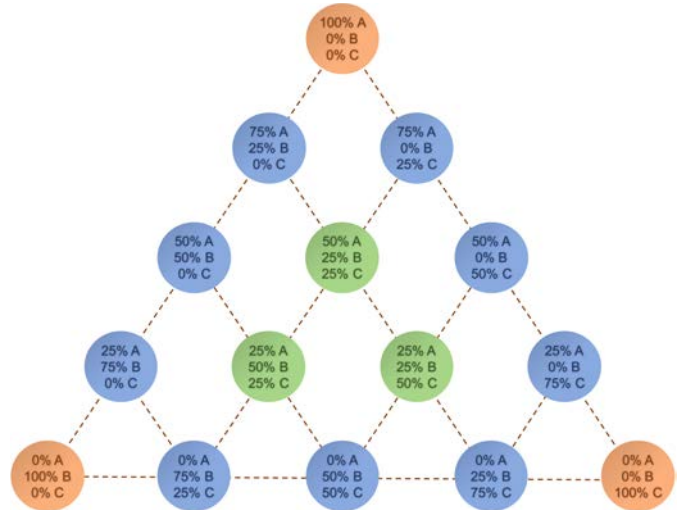


Fig. 2. Generation of synthetically mixed training data. Binary and ternary mixtures coefficients are calculated using mLMM. Mixture coefficients represent the mixing portions between 0% and 100% in 25% increments for the three considered endmembers. Nonlinearity orders are assigned randomly to every endmember contributing to the mixture.

orders which can be considered for the contribution of each pure spectra over each considered mixture [p_{lr} in (1)]. For the training data generation, we adopt a random nonlinearity order distribution that (combined with a proper mixture coefficient sampling) provides our methodology with sufficient representativity.

Last but not least, when dealing with real data sets, it is also highly desirable to expand the synthetically generated mixtures including noisy versions of each training pattern. For this purpose, we have used zero-mean Gaussian noise in different signal-to-noise ratios following the procedure described in [32].

III. EXPERIMENTAL RESULTS

To validate the proposed approach, tests on synthetic and real hyperspectral data were performed. All the experiments and the corresponding results are reported in the following.

A. Synthetic Data Sets

In order to evaluate the performance of the proposed methodologies, we have designed two different synthetic databases. The first one is a database of five 100×100 pixel synthetic hyperspectral scenes with randomly generated abundance and nonlinearity order coefficients (Random 1–Random 5). It should be noted that these data do not contain meaningful spatial information, which is not the typical situation in real hyperspectral data sets. Therefore, we have also designed a second set of five 100×100 pixel synthetic hyperspectral that have been created using fractals to generate distinct spatial patterns (Fractal 1–Fractal 5). Several natural objects can be approximated by fractals to a certain degree, including clouds, mountain ranges, coastlines, vegetation areas, etc., thus providing a baseline for simulating

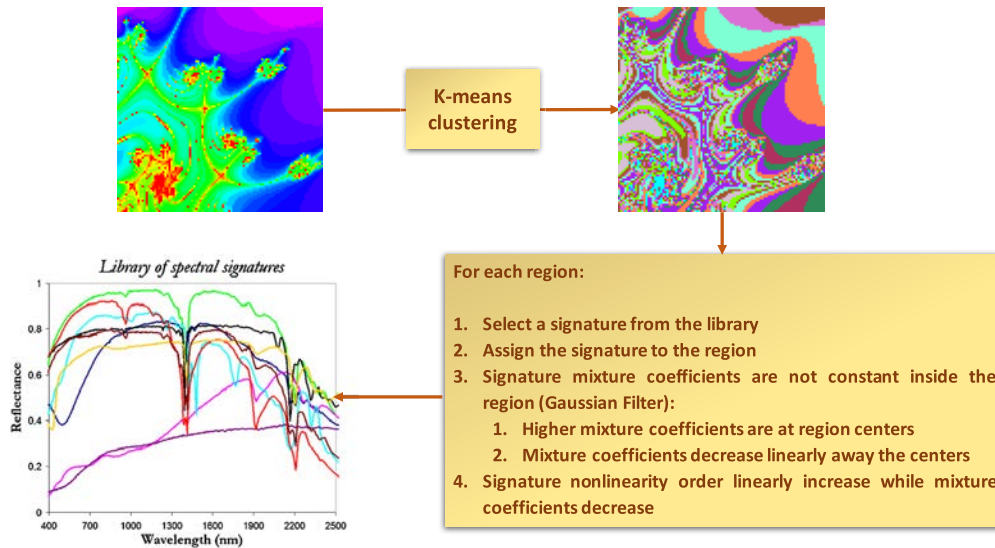


Fig. 3. Block diagram describing our procedure for generating synthetic hyperspectral images based on the mpLMM, as described in Section III-A.

spatial patterns often found in nature. In this paper, we used fractals to simulate the linear mixtures of a set of endmember signatures randomly selected from a spectral library compiled by the U.S. Geological Survey (USGS)¹ and made up of a total of 420 signatures (see Fig. 3). Fig. 4 displays the five fractal images used in the simulations. These images are further divided into a number of clusters using the k -means algorithm [33], where the number of clusters extracted from the five fractal images was always larger than the number of endmember signatures, fixed in our experiments to $p = 9$.

A crucial step in the simulation procedure is how to assign a spectral signature to each cluster. For this purpose, we have implemented an automatic procedure that follows a simple strategy in which the $p = 9$ signatures are first assigned to spatially disjoint regions belonging to different clusters. The remaining regions are then assigned spectral signatures in an automatic way, ensuring that: 1) spatially adjacent clusters always have different signatures associated with them and 2) there is a balance among the overall number of pixels in the image which are associated with each spectral signature. Inside each region, the abundance proportions of spectral signatures have been generated following a procedure that tries to imitate reality as much as possible, i.e., those pixels closer to the borders of the regions are more heavily mixed, while the pixels located at the center of the regions are more spectrally pure in nature. This is accomplished by mixing the signature associated with each cluster with those associated with neighboring clusters, making sure that the most spectrally pure signature remains at the center of the region while signature purity decreases linearly away from the center to the borders of the regions. For this purpose, a Gaussian filter is applied where the width of the Gaussian is carefully adjusted according to the width of each window. With the aforementioned procedure which is graphically illustrated by

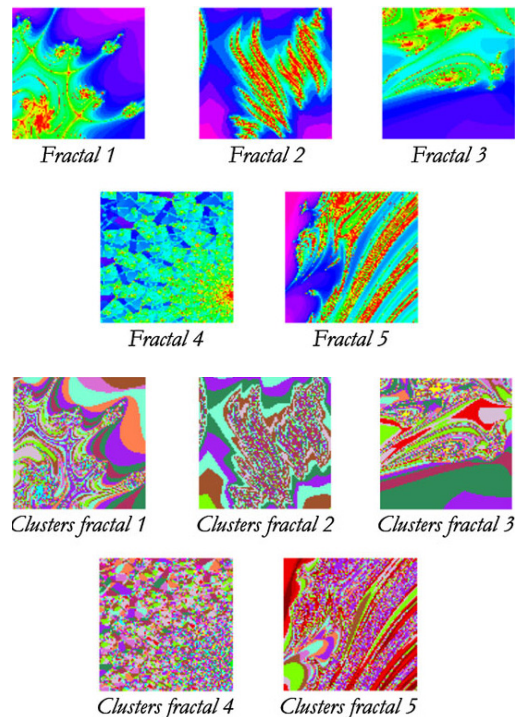


Fig. 4. Synthetic images, where spatial patterns for the mixture coefficients were (Left) generated using fractals then (Right) segmented into clusters. The generation of these patterns follows the guidelines described in Section III-A.

a block diagram in Fig. 2, the simulated regions exhibit the following properties.

- 1) All the simulated pixels inside a region are mixed, and the simulated image does not contain completely pure pixels. This increases the complexity of the unmixing problem and simulates the situation often encountered in real-world analysis scenarios, in which completely pure pixels are rarely found.
- 2) Pixels close to the borders of the region are more heavily mixed than those in the center of the region.

¹<http://speclab.cr.usgs.gov/spectral-lib.htm>

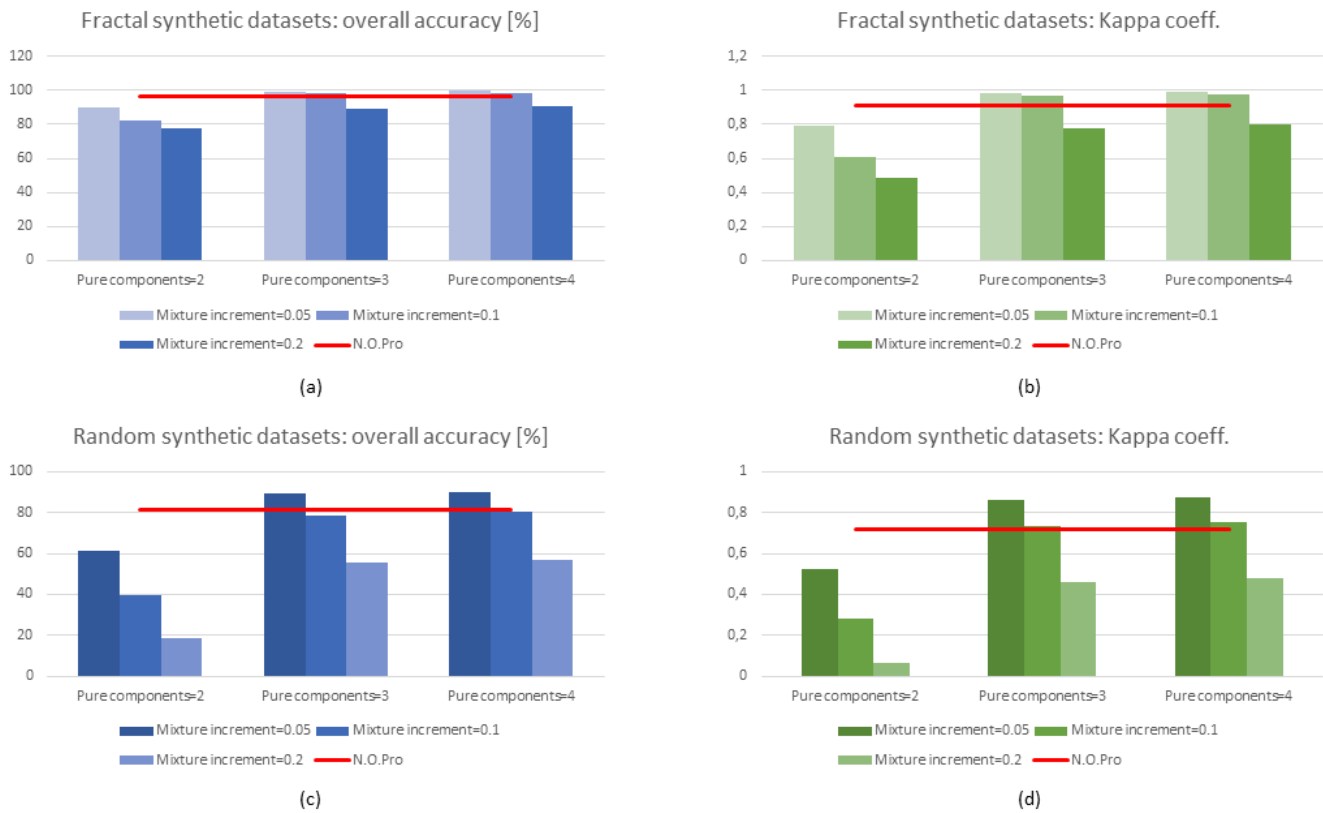


Fig. 5. Nonlinearity estimation results obtained over the synthetic data sets generated according to (a) and (b) fractal patterns and (c) and (d) random patterns. Performances are evaluated in terms of overall accuracy and Kappa coefficient. Bars: outcomes achieved by different settings of the method in Section II-B. Red solid lines: results provided by the framework in Section II-A.

- 3) If the simulated region is sufficiently large, the pixels located at the center can exhibit a degree of purity of 99% of a certain endmember. However, if the size of the simulated region is small, the degree of purity of pixels at the center of the region can decrease until 95% of a certain endmember, while pixels located in the region borders are generally more heavily mixed.
- 4) The nonlinearity orders are set so that those pixels that are more heavily mixed have larger nonlinearity orders, while more spectrally pure pixels have lower nonlinearity orders in their mixtures.

Fig. 3 illustrates the procedure for generating one of the synthetic hyperspectral scenes (labeled as “Fractal 1” in Fig. 4). The results obtained are summarized in Fig. 5, which includes the overall accuracy and Kappa coefficient. The Kappa coefficient is defined as a function of the confusion matrix that is achieved. In detail, let us assume that the counts of true positives, true negatives, false positives, and false negatives are listed as TP, TN, FP, and FN, respectively. Then, the Kappa coefficient is defined as $\kappa = (p_o - p_e) / (1 - p_e)$, where $p_o = (TP + TN) / (TP + TN + FP + FN)$ and $p_e = (\alpha + \beta) / (TP + TN + FP + FN)$. Moreover, $\alpha = [(TP + FN) \cdot (TP + FP)] / (TP + TN + FP + FN)$ and $\beta = [(FP + TN) \cdot (TN + FN)] / (TP + TN + FP + FN)$. Accordingly, the overall accuracy is defined as $(TP + TN) / (TP + FN + TN + FP)$. The outcomes achieved by different settings (i.e., number of pure components and percentage of mixture increment) of the method in Section II-B are displayed as bars, whilst the results provided by the framework in Section II-A are shown as red solid lines. The obtained estimates show that the architecture introduced in Section II-A is typically able to track and quantify the nonlinear contributions delivered by each endmember to the considered scene. Furthermore, the tests that have been carried out by different settings of the architecture in Section II-B show that it can actually provide very accurate estimates of the nonlinearity orders. Indeed, it is possible to appreciate that the actual improvement delivered by increasing the number of pure components to be used within the ANN scheme (mixing complexity) is very tiny when the order is greater than 3. Mixture coefficient sampling has a larger impact on the results. It can be seen in Fig. 5 that the lowest mixture increments the highest estimation accuracy (best results are achieved using a mixture increment of 0.05, which means that we generate 20 training patterns of a simple binary mixture). Summarizing our experiments with synthetic data indicate that the proposed ANN-based framework for estimation of nonlinearity orders according to mpLMM can deliver precise outcomes with a low computational complexity cost at the same time. Moreover, the proposed scheme for enhanced definition of hyperspectral mixture model provides a thorough characterization of scene composition, since abundance distribution can be accurately estimated by precise determination of the nonlinear contributions.

components and percentage of mixture increment) of the method in Section II-B are displayed as bars, whilst the results provided by the framework in Section II-A are shown as red solid lines. The obtained estimates show that the architecture introduced in Section II-A is typically able to track and quantify the nonlinear contributions delivered by each endmember to the considered scene. Furthermore, the tests that have been carried out by different settings of the architecture in Section II-B show that it can actually provide very accurate estimates of the nonlinearity orders. Indeed, it is possible to appreciate that the actual improvement delivered by increasing the number of pure components to be used within the ANN scheme (mixing complexity) is very tiny when the order is greater than 3. Mixture coefficient sampling has a larger impact on the results. It can be seen in Fig. 5 that the lowest mixture increments the highest estimation accuracy (best results are achieved using a mixture increment of 0.05, which means that we generate 20 training patterns of a simple binary mixture). Summarizing our experiments with synthetic data indicate that the proposed ANN-based framework for estimation of nonlinearity orders according to mpLMM can deliver precise outcomes with a low computational complexity cost at the same time. Moreover, the proposed scheme for enhanced definition of hyperspectral mixture model provides a thorough characterization of scene composition, since abundance distribution can be accurately estimated by precise determination of the nonlinear contributions.

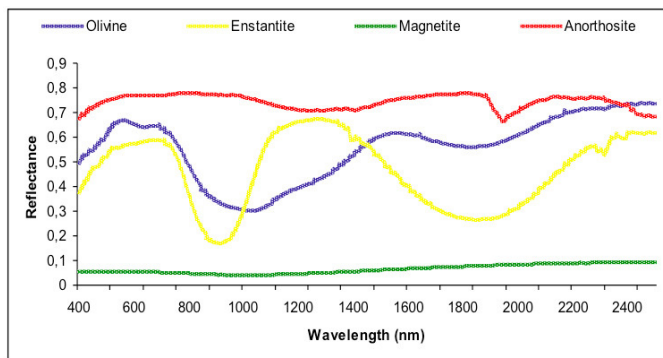


Fig. 6. Spectral signatures of magnetite, enstatite, anorthosite, and olivine in ReLab data set described in Section III-B1.

B. Real Data Sets

1) *ReLab Data*: We have also applied the methods in Section II to a data set with real spectra collected from nonlinear mixtures. These data, provided by Prof. John Mustard at Brown University, consisted of a set of spectral signatures collected using the ReLab spectrometer (a high-resolution, bidirectional spectrometer at Brown University). The ReLab data set has been constructed by using 22 spectral signatures characterized by 211 bands in the 400–2500 nm range. These records result from different mixtures of four minerals, namely, magnetite, enstatite, anorthosite, and olivine (see Fig. 6). Specifically, the data set consists of 16 spectra resulting of mixtures of two endmembers and six signatures obtained from mixing three endmembers.

In order to evaluate the consistency of the results achieved by our newly introduced methods, we computed the spectral angle distance (SAD) [30] between the nonlinearity order estimates provided by both of them. Hence, when SAD tends to 0, it means that the estimates achieved by the two methods are coherent; on the contrary, when SAD tends to 90° , the nonlinearity order estimates are completely divergent. Fig. 7 shows a radar plot of the SAD between the estimates of the nonlinearity orders of each endmember in the ReLab data set achieved by means of the methods in Section II. The SAD distribution obtained over the spectra resulting from mixtures of two and three endmembers are shown in blue and orange solid lines, respectively. The vertices of those curves show the achieved SAD value for each endmember. It is possible to appreciate that the two methods we considered deliver very consistent performance. Specifically, the resulting estimates are very similar when the spectra resulting from mixtures of two endmembers are considered. Moreover, the lowest correlation factor that has been achieved shows up when considering the magnetite mineral. It is worth noting that magnetite is characterized by octahedral crystal structure where fractures are typically uneven. These properties lead to reflectance contributions living in a higher order nonlinearity spectral domain at a macroscopic scale. Thus, mixtures involving magnetite might have been better tracked by extending the analysis to higher nonlinearity orders, so that more accurate description of the mpLMM composition could be retrieved.

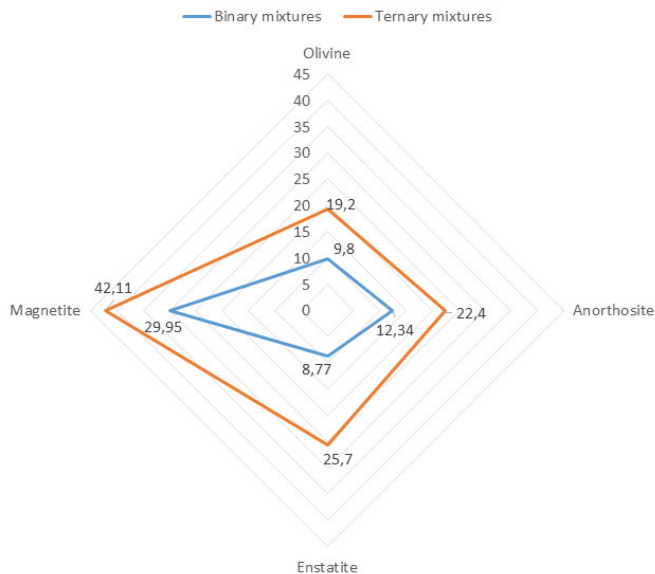


Fig. 7. Radar plot of the SAD (in degrees) between the estimates of the nonlinearity orders of each endmember in the ReLab data set achieved by means of the methods in Section II: Blue solid lines: results over the spectra identifying mixtures of two endmembers. Orange solid lines: results over the spectra identifying mixtures of three endmembers.

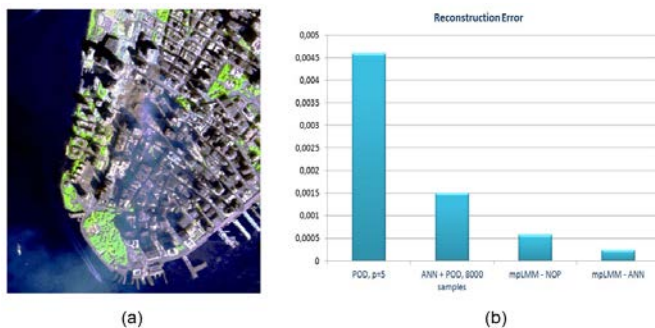


Fig. 8. (a) Red-green-blue composite of the WTC image and (b) RE performance as delivered by the POD method, the ANN+POD architecture [11], and the proposed approach based on mpLMM as considered by the methods in Section II-A and II-B.

2) *AVIRIS Data*: Finally, we tested our new techniques using a real hyperspectral image collected over the World Trade Center area in New York City [see Fig. 8(a)]. The image was obtained by the AVIRIS instrument on September 16, 2001, just 5 days after the terrorist attacks that collapsed the two main towers and other buildings in the WTC area. The full data set considered consists on 614×507 pixels, with $N = 224$ bands, and a spatial resolution of 1.7 m/pixel. Fig. 8(a) shows a false color composite of the area using the 1.682, 1.107, and 655-nm channels, displayed as red, green, and blue, respectively. Extensive reference information, collected by the USGS, is available for the WTC scene. To be consistent with the analysis we have performed in [11], 10 endmembers of the WTC scene have been extracted using the orthogonal subspace projection algorithm [29].

Fig. 8(b) reports the reconstruction error (RE) performance [defined as $RE = ((1/PN) \sum_{l=1}^P \|\underline{y}_l - \hat{\underline{y}}_l\|^2)^{1/2}$ and $\hat{\underline{y}}_l$ identifies the reconstructed spectral signature of the l th pixel

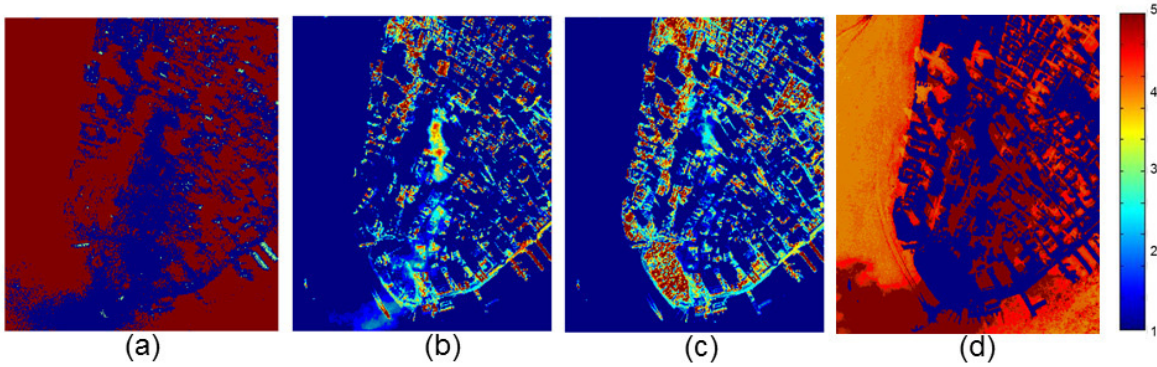


Fig. 9. (a) Nonlinearity order as estimated by the scheme in [11] on each pixel of the WTC image. (b), (c), and (d) Nonlinearity orders estimated by the method in Section II-A for three endmembers over the same image.

obtained by means of unmixing] as provided over the WTC image by the polytope decomposition (POD) method, ANN+POD architecture [11], and the proposed algorithms based on mpLMM. Specifically, according to the investigation we have performed in [11], POD has been used when the hyperspectral mixture is modeled by means of a five-LMM. In the case of mpLMM+ANN, the synthetic training was generated using three pure components on each mixture with an increment of 0.05 and the maximum nonlinearity order considered was 5. On the other hand, the nonlinearity order used to unmix each pixel according to the ANN+POD scheme is set as described in Fig. 9(a). Finally, Fig. 9(b)–(d) reports the nonlinearity orders of three endmembers over each pixel as estimated by means of the proposed approach. Moreover, the maximum value of nonlinearity that has been discovered by the proposed framework is 5.

From a computational viewpoint, the mpLMM+ANN results have been obtained in 550.02 s (synthetic data generation for 5 different simulations: 13.67 s; 5 repetitions of the training and test process: 535.56 s; ensemble of the 5 results: 0.79 s). These results have been obtained on a MacBook Pro 2.3-GHz Intel Core i5, 16-GB 2133-MHz LPDDR3 laptop. On the other hand, the mpLMM+NOPro tests have been carried out using a 2.6-GHz, 64-bit Intel Core i7-4510U CPU 16-GB RAM laptop, and have been obtained in 792 s. It is worth noting, however, that the computational efficiency of the proposed frameworks was beyond the scope of this paper. Indeed, it is possible to foresee that more efficient performance of the considered algorithms can be achieved by taking advantage of the geometrical properties (Section II-A) and the convolutional processing (Section II-B) within properly configured high performance computing platforms [34]. Hence, the execution times could be further decreased so that the computational complexity of the proposed architectures can be further leveraged and reduced.

Our results based on the RE show that the proposed approach is actually able to outperform the other higher order nonlinear hyperspectral unmixing architectures that have been introduced in [11]. Apparently, the proposed algorithm is able to accurately detect the nonlinearities over the image. Moreover, the method proposed in Section II-A aims at avoiding the local overfitting provided by the p -LMM when a higher nonlinearity order is applied to endmembers that poorly

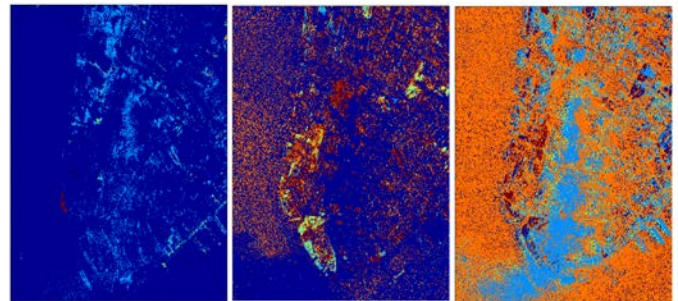


Fig. 10. Nonlinearity orders estimated by the method in Section II-B for three endmembers over the WTC image. The same colormap as in Fig. 9 applies here.

contribute to the overall nonlinear combinations which occur over each pixel (see Fig. 9). Thus, the proposed approach can be actually used for enhancing higher order nonlinear hyperspectral unmixing by an accurate detection of the nature of the reflectance combinations occurring over the considered image. Furthermore, Fig. 10 reports the nonlinearity order estimates obtained over three endmembers according to the algorithm in Section II-B. Apparently, the obtained nonlinearity estimates are a little less smooth than those retrieved by the method in Section II-A. This effect might be caused by the geometrical complexity of the scenes, where the urban environment was affected by fires contribution as well. This situation, together with the lack of ground truth available on the area, can jeopardize the performance of the architecture in Section II-B, as the ANN can be not effectively be trained. However, it is also possible to appreciate that the architecture for nonlinearity order estimation based on ANN is able to outperform the other considered methods in terms of RE (Fig. 8).

IV. CONCLUSION

In this paper, two new methods have been developed for accurately estimating the nonlinear contributions within hyperspectral mixtures. One of the methods relies on exploiting geometrical features of hyperspectral signatures in terms of nonorthogonal projections onto the space induced by the endmembers' spectra. Another method uses an ANN-based approach for nonlinearity order estimation. Both methods aim at providing a precise estimation of the order of nonlinearity that characterizes the combinations of endmember recorded

by each pixel spectrum. The proposed architectures aim at understanding the order of local nonlinearity that is displayed by each endmember over every pixel by projecting every quantity in the unmixing formula onto the space spanned by the given endmember set, and by learning the nonlinearity orders according to a properly designed neural network, respectively. The main contributions of this paper are:

- 1) the introduction of a novel mixture model that is able to outline the actual nonlinear contributions delivered by the interactions among endmembers;
- 2) the development of a new scheme for efficient description of the nonlinear combinations of endmembers based on nonorthogonal projections; and
- 3) the design of a novel approach for characterization of the nonlinearity distribution over each pixel developed according to a neural network learning framework.

Our experimental results, conducted using a variety of synthetic and real hyperspectral data sets, show that the proposed approaches are actually able to retrieve thorough information on the nature of the nonlinear effects while providing excellent performance in reconstructing the given data sets. In the future, we plan to develop computationally efficient implementations of the proposed methods using a variety of high-performance computing architectures.

ACKNOWLEDGMENT

This paper represents an enhanced version of A. Marinoni, J. Plaza, A. Plaza and, P. Gamba, "An iterative enhancement of higher order nonlinear mixture model for accurate hyperspectral unmixing," presented at IEEE WHISPERS 2016, Los Angeles, CA USA.

REFERENCES

- [1] R. Heylen, M. Parente, and P. Gader, "A review of nonlinear hyperspectral unmixing methods," *IEEE J. Sel. Topics Appl. Earth Observ. Remote Sens.*, vol. 7, no. 6, pp. 1844–1868, Jun. 2014.
- [2] N. Dobigeon, J.-Y. Tourneret, C. Richard, J. C. M. Bermudez, S. McLaughlin, and A. O. Hero, "Nonlinear unmixing of hyperspectral images: Models and algorithms," *IEEE Signal Process. Mag.*, vol. 31, no. 1, pp. 82–94, Jan. 2014.
- [3] J. M. Bioucas-Dias *et al.*, "Hyperspectral unmixing overview: Geometrical, statistical, and sparse regression-based approaches," *IEEE J. Sel. Topics Appl. Earth Observ. Remote Sens.*, vol. 5, no. 2, pp. 354–379, Apr. 2012.
- [4] A. Marinoni and P. Gamba, "A novel approach for efficient p -linear hyperspectral unmixing," *IEEE J. Sel. Topics Signal Process.*, vol. 9, no. 6, pp. 1156–1168, Sep. 2015.
- [5] A. Marinoni, A. Plaza, and P. Gamba, "Harmonic mixture modeling for efficient nonlinear hyperspectral unmixing," *IEEE J. Sel. Topics Appl. Earth Observ. Remote Sens.*, vol. 9, no. 9, pp. 4247–4256, Sep. 2016.
- [6] R. Heylen and P. Gader, "Nonlinear spectral unmixing with a linear mixture of intimate mixtures model," *IEEE Geosci. Remote Sens. Lett.*, vol. 11, no. 7, pp. 1195–1199, Jul. 2014.
- [7] R. Close, P. Gader, J. Wilson, and A. Zare, "Using physics-based macroscopic and microscopic mixture models for hyperspectral pixel unmixing," *Proc. SPIE*, vol. 8390, p. 83901L, Apr. 2012.
- [8] B. Broadwater, R. Chellappa, A. Banerjee, and P. Burlina, "Kernel fully constrained least squares abundance estimates," in *Proc. IEEE Int. Geosci. Remote Sens. Symp. (IGARSS)*, Barcelona, Spain, Jul. 2007, pp. 4041–4044.
- [9] A. Marinoni and P. Gamba, "Accurate detection of anthropogenic settlements in hyperspectral images by higher order nonlinear unmixing," *IEEE J. Sel. Topics Appl. Earth Observ. Remote Sens.*, vol. 9, no. 5, pp. 1792–1801, May 2016.
- [10] I. Meganem, P. Deliot, X. Briottet, Y. Deville, and S. Hosseini, "Linear-quadratic mixing model for reflectances in urban environments," *IEEE Trans. Geosci. Remote Sens.*, vol. 52, no. 1, pp. 544–558, Jan. 2014.
- [11] A. Marinoni, J. Plaza, A. Plaza, and P. Gamba, "Nonlinear hyperspectral unmixing using nonlinearity order estimation and polytope decomposition," *IEEE J. Sel. Topics Appl. Earth Observ. Remote Sens.*, vol. 8, no. 6, pp. 2644–2654, Jun. 2015.
- [12] M.-D. Iordache, J. Bioucas-Dias, and A. Plaza, "Sparse unmixing of hyperspectral data," *IEEE Trans. Geosci. Remote Sens.*, vol. 49, no. 6, pp. 2014–2039, Jun. 2011.
- [13] Y. Zhong, R. Feng, and L. Zhang, "Non-local sparse unmixing for hyperspectral remote sensing imagery," *IEEE J. Sel. Topics Appl. Earth Observ. Remote Sens.*, vol. 7, no. 6, pp. 1889–1909, Jun. 2014.
- [14] Y. Zhong, X. Wang, L. Zhao, R. Feng, L. Zhang, and Y. Xu, "Blind spectral unmixing based on sparse component analysis for hyperspectral remote sensing imagery," *ISPRS J. Photogram. Remote Sens.*, vol. 119, pp. 49–63, Sep. 2016.
- [15] X. Wang, Y. Zhong, L. Zhang, and Y. Xu, "Spatial group sparsity regularized nonnegative matrix factorization for hyperspectral unmixing," *IEEE Trans. Geosci. Remote Sens.*, vol. 55, no. 11, pp. 6287–6304, Nov. 2017.
- [16] R. Heylen and P. Scheunders, "A multilinear mixing model for nonlinear spectral unmixing," *IEEE Trans. Geosci. Remote Sens.*, vol. 54, no. 1, pp. 240–251, Jan. 2016.
- [17] R. Ammanouil, A. Ferrari, C. Richard, and S. Mathieu, "Nonlinear unmixing of hyperspectral data with vector-valued kernel functions," *IEEE Trans. Image Process.*, vol. 26, no. 1, pp. 340–354, Jan. 2017.
- [18] A. Halimi, P. Honeine, and J. M. Bioucas-Dias, "Hyperspectral unmixing in presence of endmember variability, nonlinearity, or mismodeling effects," *IEEE Trans. Image Process.*, vol. 25, no. 10, pp. 4565–4579, Oct. 2016.
- [19] Y. Altmann, N. Dobigeon, and J.-Y. Tourneret, "Nonlinearity detection in hyperspectral images using a polynomial post-nonlinear mixing model," *IEEE Trans. Image Process.*, vol. 22, no. 4, pp. 1267–1274, Apr. 2013.
- [20] Y. Altmann, N. Dobigeon, S. McLaughlin, and J.-Y. Tourneret, "Residual component analysis of hyperspectral images—Application to joint nonlinear unmixing and nonlinearity detection," *IEEE Trans. Image Process.*, vol. 23, no. 5, pp. 2148–2158, May 2014.
- [21] Y. Altmann, N. Dobigeon, S. McLaughlin, and J.-Y. Tourneret, "Unsupervised post-nonlinear unmixing of hyperspectral images using a Hamiltonian Monte Carlo algorithm," *IEEE Trans. Image Process.*, vol. 23, no. 6, pp. 2663–2675, Jun. 2014.
- [22] A. Marinoni, A. Plaza, and P. Gamba, "A novel preunmixing framework for efficient detection of linear mixtures in hyperspectral images," *IEEE Trans. Geosci. Remote Sens.*, vol. 55, no. 8, pp. 4325–4333, Aug. 2017.
- [23] I. N. Herstein, *Topics in Algebra*, 2nd ed. Hoboken, NJ, USA: Wiley, 1975.
- [24] R. Heylen, D. Burazerovic, and P. Scheunders, "Non-linear spectral unmixing by geodesic simplex volume maximization," *IEEE J. Sel. Topics Signal Process.*, vol. 5, no. 3, pp. 534–542, Jun. 2011.
- [25] K. Hornik, "Approximation capabilities of multilayer feedforward networks," *Neural Netw.*, vol. 4, no. 2, pp. 251–257, 1991.
- [26] M. F. Møller, "A scaled conjugate gradient algorithm for fast supervised learning," *Neural Netw.*, vol. 6, no. 4, pp. 525–533, Nov. 1993.
- [27] A. Okujeni, S. van der Linden, S. Suess, and P. Hostert, "Ensemble learning from synthetically mixed training data for quantifying urban land cover with support vector regression," *IEEE J. Sel. Topics Appl. Earth Observ. Remote Sens.*, vol. 10, no. 4, pp. 1640–1650, Apr. 2017, doi: 10.1109/JSTARS.2016.2634859.
- [28] S. Suess, S. van der Linden, P. J. Leitao, A. Okujeni, B. Waske, and P. Hostert, "Import vector machines for quantitative analysis of hyperspectral data," *IEEE Geosci. Remote Sens. Lett.*, vol. 11, no. 2, pp. 449–453, Feb. 2014.
- [29] H. Ren and C.-I. Chang, "Automatic spectral target recognition in hyperspectral imagery," *IEEE Trans. Aerosp. Electron. Syst.*, vol. 39, no. 4, pp. 1232–1249, Oct. 2003.
- [30] C.-I. Chang and Q. Du, "Estimation of number of spectrally distinct signal sources in hyperspectral imagery," *IEEE Trans. Geosci. Remote Sens.*, vol. 42, no. 3, pp. 608–619, Mar. 2004.
- [31] R. A. Schowengerdt, *Remote Sensing: Models and Methods for Image Processing*, 3rd ed. New York, NY, USA: Academic, 1997.
- [32] J. C. Harsanyi and C.-I. Chang, "Hyperspectral image classification and dimensionality reduction: An orthogonal subspace projection approach," *IEEE Trans. Geosci. Remote Sens.*, vol. 32, no. 4, pp. 779–785, Jul. 1994.
- [33] J. A. Hartigan and M. A. Wong, "Algorithm AS 136: A K -means clustering algorithm," *J. Roy. Stat. Soc.*, vol. 28, no. 1, pp. 100–108, 1979.
- [34] A. Plaza and C. Chang, *High Performance Computing in Remote Sensing*. Boca Raton, FL, USA: CRC Press, 2007.



Andrea Marinoni (S'07–M'11–SM'16) received the B.S., M.Sc. (*cum laude*), and Ph.D. degrees in electronic engineering from the University of Pavia, Pavia, Italy, in 2005, 2007, and 2011, respectively.

In 2009, he was a Visiting Researcher with the Communications Systems Laboratory, Department of Electrical Engineering, University of California at Los Angeles, Los Angeles, CA, USA. Since 2013, he has been a Research Fellow with the Telecommunications and Remote Sensing Laboratory, Department of Electrical, Computer, and Biomedical Engineering, University of Pavia. From 2015 to 2017, he was a Visiting Researcher with the Earth and Planetary Image Facility, Ben-Gurion University of the Negev, Beersheba, Israel; the School of Geography and Planning, Sun Yat-sen University, Guangzhou, China; the School of Computer Science, Fudan University, Shanghai, China; the Institute of Remote Sensing and Digital Earth, Chinese Academy of Sciences, Beijing, China; and the Instituto de Telecomunicacoes, Instituto Superior Tecnico, Universidade de Lisboa, Lisbon, Portugal. His research interests include efficient nonlinear signal processing applied to multimodal remote sensing, Earth observation interpretation, and Big Data mining, analysis, and management for human-environment interaction assessment.

Dr. Marinoni was a recipient of the two-year Applied research grant, sponsored by the Region of Lombardy, Italy, and STMicroelectronics N.V. in 2011, the INROAD grant, sponsored by the University of Pavia and Fondazione Cariplo, Italy, for supporting excellence in design of ERC proposal, in 2017, the Progetto professionalità Ivano Becchi grant funded by Fondazione Banco del Monte di Lombardia, Italy, and sponsored by the University of Pavia and NASA Jet Propulsion Laboratory, Pasadena, CA, USA, for supporting the development of advanced methods of air pollution analysis by remote sensing data investigation, in 2018. He serves as a reviewer for several major journals and conferences sponsored by the IEEE Geoscience and Remote Sensing Society, the IEEE Communications Society, the IEEE Signal Processing Society, the IEEE Information Theory Society, the International Association of Pattern Recognition, the International Society on Urban Health, and the American Medical Informatics Association. He has been an invited speaker at the 2010 Workshop on Application of Communication Theory to Emerging Memory Technologies, IEEE Global Communications conference, Miami, FL, USA, the 2014 New Challenges in Astro- and Environmental Informatics in the Big Data Era Workshop, Szombathely, Hungary, Big Data Methodologies in Remote Sensing and Astronomy special session at the 2015 IEEE Geoscience and Remote Sensing Symposium, Milan, Italy, and the 2015 Astroinformatics, Dubrovnik, Croatia.



Javier Plaza (M'09–SM'15) received the M.Sc. and Ph.D. degrees in computer engineering from the Hyperspectral Computing Laboratory, Department of Technology of Computers and Communications, University of Extremadura, Badajoz, Spain, in 2004 and 2008, respectively.

He is currently a member of the Hyperspectral Computing Laboratory. He has authored over 150 publications, including over 50 journal citation reports (JCR) journal papers, 10 book chapters, and 90 peer-reviewed conference proceeding papers. He has guest edited four special issues on hyperspectral remote sensing for different journals. His research interests include hyperspectral data processing and parallel computing of remote sensing data.

Dr. Plaza was a recipient of the Outstanding Ph.D. Dissertation Award at the University of Extremadura in 2008, the Best Column Award of IEEE *Signal Processing Magazine* in 2015, the Most Highly Cited Paper in the *Journal of Parallel and Distributed Computing*, from 2005 to 2010, and the Best Paper Awards with the IEEE International Conference on Space Technology and the IEEE Symposium on Signal Processing and Information Technology. He is currently an Associate Editor with IEEE GEOSCIENCE AND REMOTE SENSING LETTERS and the IEEE Remote Sensing Code Library.



Antonio Plaza (M'05–SM'07–F'15) received the M.Sc. and Ph.D. degrees in computer engineering from the Department of Technology of Computers and Communications, University of Extremadura, Badajoz, Spain.

He is currently the Head of the Hyperspectral Computing Laboratory, Department of Technology of Computers and Communications, University of Extremadura. He has authored more than 500 publications, including 193 JCR journal papers (over 140 in the IEEE journals), 23 book chapters, and 285 peer-reviewed conference proceeding papers. He has guest edited 10 special issues on hyperspectral remote sensing for different journals, and has reviewed more than 500 manuscripts for over 50 different journals. His research interests include hyperspectral data processing and parallel computing of remote sensing data.

Dr. Plaza was a recipient of the Recognition of Best Reviewers of IEEE GEOSCIENCE AND REMOTE SENSING LETTERS in 2009 and the Recognition of Best Reviewers of the IEEE TRANSACTIONS ON GEOSCIENCE AND REMOTE SENSING in 2010, the Best Column Award of IEEE *Signal Processing Magazine* in 2015, the 2013 Best Paper Award of the IEEE JOURNAL OF SELECTED TOPICS IN APPLIED EARTH OBSERVATIONS AND REMOTE SENSING, the Most Highly Cited Paper from 2005 to 2010 in the *Journal of Parallel and Distributed Computing*, and the Best Paper Awards at the IEEE International Conference on Space Technology and the IEEE Symposium on Signal Processing and Information Technology. He was a member of the Editorial Board of the IEEE Geoscience and Remote Sensing Newsletter from 2011 to 2012 and IEEE GEOSCIENCE AND REMOTE SENSING MAGAZINE in 2013. He was also a member of the steering committee of the IEEE JSTARS. He was as the Director of Education Activities for the IEEE Geoscience and Remote Sensing Society (GRSS) from 2011 to 2012, and is currently a President of the Spanish Chapter of IEEE GRSS. He was an Associate Editor of the IEEE TRANSACTIONS ON GEOSCIENCE AND REMOTE SENSING from 2007 to 2012. He is an Associate Editor of the IEEE ACCESS. He is the former Editor-in-Chief for the IEEE TRANSACTIONS ON GEOSCIENCE AND REMOTE SENSING.



Paolo Gamba (SM'00–F'13) received the Laurea (*cum laude*) and Ph.D. degrees in electronic engineering from the University of Pavia, Pavia, Italy, in 1989 and 1993, respectively.

He is currently a Professor of telecommunications with the University of Pavia, where he leads the Telecommunications and Remote Sensing Laboratory and serves as a Deputy Coordinator of the Ph.D. School in Electronics and Computer Science. He has been invited to give keynote lectures and tutorials in several occasions about urban remote sensing, data fusion, EO data and risk management. He has authored or co-authored more than 130 papers in international peer-review journals and presented more than 250 research works in workshops and conferences.

Dr. Gamba has been the organizer and Technical Chair of the biennial GRSS/ISPRS Joint Workshops on "Remote Sensing and Data Fusion over Urban Areas" since 2001. He also served as Technical Co-Chair of the 2010 and 2015 IGARSS conferences, in Honolulu (Hawaii), and Milan (Italy), respectively. He was the Chair of the Data Fusion Committee of the IEEE Geoscience and Remote Sensing Society from 2005 to 2009. He serves as a GRSS Vice President for Professional Activities, the Chair of the Chapters Committee, the Chair of the Symposium Awards Committee. He was the Editor-in-Chief of IEEE GEOSCIENCE AND REMOTE SENSING LETTERS from 2009 to 2013.

He has been the Guest Editor of special issues of IEEE TRANSACTIONS ON GEOSCIENCE AND REMOTE SENSING, the IEEE JOURNAL OF SELECTED TOPICS IN REMOTE SENSING APPLICATIONS, the *ISPRS Journal of Photogrammetry and Remote Sensing*, the *International Journal of Information Fusion*, and the *Pattern Recognition Letters on the topics of Urban Remote Sensing, Remote Sensing for Disaster Management, Pattern Recognition in Remote Sensing Applications*.